Coherence dynamics and quantum-to-classical crossover in an exciton–cavity system in the quantum strong coupling regime

Coherence dynamics and quantum-to-classical crossover in an exciton–cavity system in the quantum strong coupling regime

J Kasprzak[1,5], **K Sivalertporn**[2], **F Albert**[3], **C Schneider**[3],
S Höfling[3], **M Kamp**[3], **A Forchel**[3], **S Reitzenstein**[3,4],
E A Muljarov[2,6] **and W Langbein**[2]

[1] Institut Néel, CNRS, BP 166, F-38042 Grenoble Cedex 9, France
[2] School of Physics and Astronomy, Cardiff University, The Parade, CF24 3AA Cardiff, UK
[3] Technische Physik, Physikalisches Institut, and Wilhelm Conrad Röntgen Research Center for Complex Material Systems, Universität Würzburg, Am Hubland, D-97074 Würzburg, Germany
[4] Institut für Festkörperphysik, Technische Universität Berlin, Hardenbergstrasse 36, D-10623 Berlin, Germany
E-mail: jacek.kasprzak@grenoble.cnrs.fr

Abstract. Interaction between light and matter generates optical nonlinearities, which are particularly pronounced in the quantum strong coupling regime. When a single bosonic mode couples to a single fermionic mode, a Jaynes–Cummings (JC) ladder is formed, which we realize here using cavity photons and quantum dot excitons. We measure and model the coherent anharmonic response of this strongly coupled exciton–cavity system at resonance. Injecting two photons into the cavity, we demonstrate a $\sqrt{2}$ larger polariton splitting with respect to the vacuum Rabi splitting. This is achieved using coherent nonlinear spectroscopy, specifically four-wave mixing, where the coherence between the ground state and the first (second) rung of the JC ladder can be interrogated for positive

[5] Author to whom any correspondence should be addressed.
[6] On leave from General Physics Institute RAS, Moscow, Russia.

(negative) delays. With increasing excitation intensity and thus rising average number of injected photons, we observe spectral signatures of the quantum-to-classical crossover of the strong coupling regime.

Contents

1. Introduction

Milestone achievements in cavity quantum electrodynamics (cQED) have just been awarded with the Nobel Prize in Physics 2012 (Serge Haroche and David J Wineland, 'for ground-breaking experimental methods that enable measuring and manipulation of individual quantum systems'). The underlying experiments were performed on individual atomic systems exploring light–matter interaction on a quantum level [1], and pushed the boundaries of our understanding of quantum mechanics, for instance by introducing quantum non-demolition measurements [2, 3]. cQED effects can now be observed also in solid state systems, which owing to their intrinsic stability are better suited for scalable technology and commercialization. The highest cooperativity is achieved in superconductive circuits working at microwave frequencies and milli-kelvin temperatures, consisting of Josephson junctions coupled to a waveguide resonator [4]. To work at optical frequencies compatible with optical fibre communication, one can employ individual optical transitions in semiconductor nanostructures—such as excitons in quantum dots (QDs)—which are coupled to the electromagnetic field of a micro-cavity. These systems operate at present in a temperature range of 10 K and have 3–6 orders of magnitude lower volume than superconductive circuits.

In the strong coupling regime of light and matter, excitation is reversibly and coherently exchanged between photonic modes and matter. Such a temporal 'ping-pong' corresponds to the formation of hybrid eigenstates called polaritons [5]. Strong coupling was first observed for large ensembles of matter states [6–8] within an optical resonator. The experimental evidence for strong coupling and polariton formation is a spectral anti-crossing when the relative frequencies of light and matter modes are tuned, with a vacuum Rabi splitting Ω at resonance, related to the oscillation period of exchange between light and matter of $2\pi/\Omega$.

When photons interact with a matter mode with weak self-interaction compared with the dissipation, the anharmonicity due to a single excitation is negligible and the mode is effectively bosonic [6, 7]. Conversely, if the matter mode has a strong self-interaction compared to the

dissipation, it constitutes an effective fermionic mode. In this case a Jaynes–Cummings (JC) ladder of states forms, with a splitting of $\sqrt{n}\Omega$ of the nth rung of the ladder carrying n excitation quanta. The period of the temporal oscillation is accordingly $2\pi/(\sqrt{n}\Omega)$ and shortens in discrete steps, so that going from $n = 1$ to 2 the period is reduced by a factor of $\sqrt{2}$. The discrete change of the splitting is a principal and profound result of cQED described by the JC Hamiltonian [9] and is a signature of the quantum strong coupling regime (QSC). This manifestation of QSC was first observed in atomic physics [1] and recently demonstrated in superconducting qubits strongly coupled to waveguide resonators [4, 10], where a large splitting to linewidth ratio of 260 allowed to observe up to six rungs of the ladder. Both the experiments used photonic modes in the microwave frequency range.

Solid state systems in the optical frequency regime showing QSC are at present employing semiconductor quantum dots embedded in optical cavities formed by the host semiconductor, such as photonic crystal cavities [11–13], microdiscs [14] or micropillars [15, 16]. These systems exhibit at present a modest splitting to linewidth ratio of around 2, and the spectroscopic discrimination of the discrete splitting steps is not obvious. The QSC regime was therefore indirectly demonstrated using the intensity correlation of the resonant reflection, showing a photon blockade or photon bunching [12] and single-photon switching [13]. The spectral splitting was measured directly using coherent nonlinear spectroscopy [17], specifically four-wave mixing (FWM) to probe the coherence dynamics in the first two rungs of the JC ladder [16, 18]. Recently, this technique also enabled to demonstrate the photon-mediated coherent coupling of several quantum dots in the framework of the Tavis–Cummings model [19].

In this work, we extend the investigation of the coherent response of a micropillar cavity in the QSC regime with an embedded QD reported in [16, 18]. An improved dynamic range of the data as well as a slightly better splitting to linewidth ratio of the investigated structure allowed us to retrieve the entire beat of the second rung coherence, displaying a $\sqrt{2}$ shorter period—hence $\sqrt{2}$ larger polariton splitting—with respect to the first rung. The measurements are in quantitative agreement with predictions of the FWM response based on the master equation for the density matrix of the JC ladder truncated at the second rung. Further to this, we show a continuous detuning dependence of the FWM. In the temporal domain, a continuous evolution of the beat period with a maximum at zero detuning is found. In the spectral domain, the second rung contributions lead to an apparent crossing and mixing of the transitions, while after temporal filtering, which is used in order to suppress the second rung contributions, the underlying anti-crossing can be observed. We also report on the evolution of the response with increasing average photon number n injected into the cavity mode, showing a transition from the vacuum Rabi splitting towards a semi-classical regime. In particular, with growing excitation intensity, the FWM spectra display progressively increasing influence of transitions between higher rungs of the JC ladder, yielding for large n a spectral FWM lineshape akin to a Mollow triplet.

2. The investigated sample and photoluminescence characterization

The investigated sample is similar to the one used in [19]. The fabrication process starts with the growth of a planar microcavity on a GaAs substrate by molecular beam epitaxy. A GaAs λ-cavity contains a single layer of self-assembled $In_{0.4}Ga_{0.6}As$ QDs. The vertical confinement of light is provided by two distributed Bragg reflectors, made of 26 (30) mirror pairs of $\lambda/4$ layers of GaAs and AlAs. For lateral photon confinement, micropillars were structured by means of
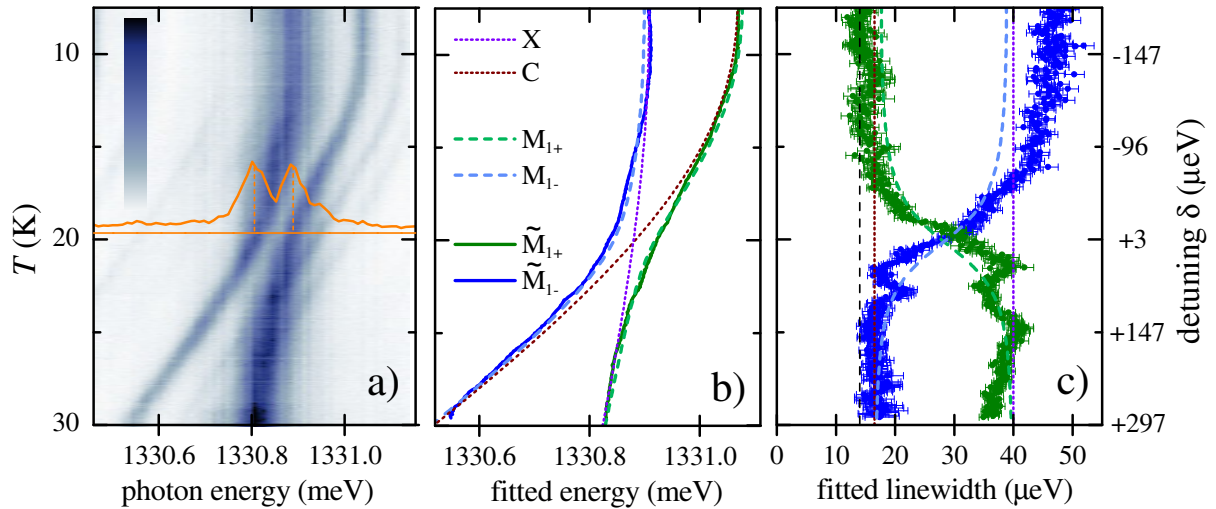
Figure 1. (a) μPL excited and collected through the top facet of the micropillar, as a function of the sample temperature. Spectral intensity on a linear colour scale from white (zero) to blue, as given. An avoided crossing between the cavity mode C and the exciton X in a QD with a Rabi splitting of $\Omega = 78\,\mu$eV is observed at $T \sim 19$ K. The μPL spectrum at this temperature is shown with baseline (orange lines). (b) Fitted spectral positions of polaritons in the first rung of the JC ladder $\tilde{M}_{1+}$ and $\tilde{M}_{1-}$ (solid green and blue lines), the resulting uncoupled states C and X (dotted violet and brown lines) and coupled states M_{1+} and M_{1-} (dashed blue and green lines). (c) Fitted linewidth (HWHM) of $\tilde{M}_{1+}$ (green) and $\tilde{M}_{1-}$ (blue) and the resulting linewidths of M_{1+}, M_{1-}, C and X using line colours and styles as in (b). The black dashed line shows spectral resolution of the measurements.

high-resolution electron beam lithography and electron cyclotron etching [20]. Fields of 6×6 micropillars of nominally equal diameter varying between 1.5 and 2.0 μm were realized. Such fields are separated by 50 μm in the x- and y-directions, corresponding to the [110] and [1$\bar{1}$0] crystallographic directions of the GaAs substrate, respectively. Each micropillar was accompanied by a reference pillar of 10 μm diameter at 10 μm distance, which was used to reflect the reference beam in the FWM experiment.

The sample was mounted on an x–y stage in a helium bath cryostat, together with a microscope objective of 0.85 numerical aperture which was adjustable in all three dimensions by a home-built stage with piezoelectric bender actuators. To identify micropillars in the strong coupling regime, we characterized them with confocal micro-photoluminescence (μPL) excited by a continuous wave laser of 532 nm wavelength, focused to a spot of about 0.5 μm full-width at half maximum (FWHM) on the top surface of the micropillar. The micropillar presented in this work was selected for high cooperativity given by the Rabi splitting to linewidth ratio. The latter crucially depends on a Q-factor of the fundamental cavity mode, which was around 21 000, corresponding to a photon lifetime of about $\tau_C = 10.5$ ps in its mode volume of approximately 0.3 μm^3. The polariton polarization decay time is therefore governed by the radiative emission and at resonance is $T_2 = 2T_1 = 4\tau_C = 42$ ps.

To characterize the exciton (X)–cavity (C) coupling, μPL spectra were measured as a function of the sample temperature from 8 to 30 K, as presented in figure 1(a). The excitation

Table 1. Parameters of the exciton-cavity system deduced from a fit to the temperature-dependent photoluminescence spectra.

Parameter	Value	Unit
$\hbar\omega_X(0)$	1331.070	meV
$\hbar\omega_C(0)$	1330.909	meV
$\hbar g$	39	μeV
$\hbar\gamma_X$	16.5	μeV
$\hbar\gamma_C$	40	μeV
α	58.05 ± 0.6	μeV K^{-1}
θ	59.31 ± 0.4	K
η	0.153297	

power at the micropillar was about 100 nW. At lower powers the PL spectrum remained essentially unchanged, while at higher powers line broadening and reduction of the Rabi splitting were observed. The PL spectrum at each temperature was fitted by a sum of two Lorentzian lines. The resulting line positions as a function of temperature show an anti-crossing (figure 1(b)) and exchange of linewidths (figure 1(c)). The pillar contains other QDs with weakly coupled excitons, which show a crossing with the strongly coupled doublet, perturbing the lineshape of the doublet by the Purcell-enhanced emission into the doublet, which for example around 23 K gives a perturbation in the fitted peak position and linewidth. The non-resonant weakly coupled QD excitons show a common temperature-dependent shift $F(T)$ which can be fitted within an explicit model of the band-gap shift of semiconductors [21]

$$F(T) = -\frac{\alpha\theta}{2}\left(\coth\left(\frac{\theta}{2T}\right) - 1\right) \tag{1}$$

using the parameters given in table 1. We assume that the cavity mode ω_C has the same shift as the exciton ω_X but scaled by a factor η,

$$\omega_X(T) = \omega_X(0) + F(T), \quad \omega_C(T) = \omega_C(0) + \eta F(T). \tag{2}$$

It is known that the PL in the strong coupling is, in general, not simply an incoherent sum of the two transitions, due to the excitation via exciton or cavity components [22, 23]. Therefore, we first determined Ω from the maximum time (corresponding to the minimum Rabi splitting at zero detuning) of the first dip in the temporal beat of the FWM response shown in figure 3(c), yielding the exciton–cavity coupling in the theoretical model of $\hbar g = 39\,\mu$eV. We then fitted the energies of the PL peaks with the calculated polariton energies of the first rung of the JC ladder, leaving as free parameters only the zero-temperature exciton $\omega_X(0)$ and cavity $\omega_C(0)$ energies and η. The resulting parameters are given in table 1, and the fit curves for the energies and linewidths are given in figures 1(b) and (c).

From the PL line of weakly coupled QD excitons and cavity, we extract the exciton linewidth half-width at half maximum (HWHM) of $\hbar\gamma_X = 16.5\,\mu$eV and the cavity linewidth (HWHM) of $\hbar\gamma_C = 40\,\mu$eV. These values include the spectrometer resolution of about $4\,\mu$eV HWHM Lorentzian and an additional $\sim5\,\mu$eV HWHM due to finite pixel size and geometrical imaging errors. Correcting for the Lorentzian part of the resolution, the cooperativity of the system is $C = g^2/\gamma_C\gamma_X \sim 3.6$, and the splitting to linewidth ratio at resonance is $2g/(\gamma_C + \gamma_X) \sim$ 1.6. The linewidth of the exciton is actually limited by spectral jitter, and the homogeneous linewidth is expected to be 2–5 μeV [24], yielding a jitter corrected cooperativity of $C \sim 10$.

Spectral anti-crossing and exchange of linewidths versus detuning $\delta = \omega_C - \omega_X$, as observed in figure 1, are generic features of any system representing coupled oscillators and do not identify QSC. To observe QSC one needs to access transitions involving higher manifolds ($n \geqslant 2$) of the JC ladder. While non-resonantly excited μPL was predicted to show some features of the QSC regime in the formation of a Mollow triplet [25], in experiments this has not been observed. This is related to the influence of the relaxation of non-resonantly excited carriers towards the QD ground state, which is often much slower than the lifetime in state-of-the-art cavities, precluding access to higher rungs and creating additional dephasing, moving the system into the weak coupling regime [26].

3. Accessing the first two rungs of the Jaynes–Cummings ladder via four-wave mixing

Exciting resonantly with an optical pulse, one can instantaneously inject n photons into the cavity mode, reaching the nth manifold of the JC ladder, with precise timing and without introducing additional dephasing mechanisms. Hence, in order to reveal the QSC regime we have chosen a resonant excitation scheme. To distinguish the response of the cavity from non-resonant reflection and to access one- and two-photon coherences, we employ FWM detected by the heterodyne spectral interferometry technique [17]. We use two trains of laser pulses $\mathcal{E}_1$ and $\mathcal{E}_2$ with a repetition rate of $\tau_r^{-1} = 76$ MHz, which are spectrally centred at the transition energies of the polaritons around 1331 meV. The pulse spectral width was 2 meV (FWHM) and the pulse duration was 0.9 ps. $\mathcal{E}_1$ and $\mathcal{E}_2$ are collinear and propagate in the same spatial mode, and are focused onto the top of the micropillar using the same optics as described above for the μPL experiment. An efficient coupling to the intra-cavity field is achieved by matching the waist of the focus with the cavity mode at the top facet of the micropillar. We up-shift the frequencies of $\mathcal{E}_1$ and $\mathcal{E}_2$ by acousto-optic modulators driven at $\Omega_1/(2\pi) = 79$ MHz and $\Omega_2/(2\pi) = 80.77$ MHz. This introduces the phase shifts $e^{i\Omega_1 m \tau_r}$ and $e^{i\Omega_2 m \tau_r}$ for the mth pulse in $\mathcal{E}_1$ and $\mathcal{E}_2$, respectively. The induced degenerate FWM signal, specifically the third-order optical polarization $P \propto \mathcal{E}_1^* \mathcal{E}_2^2$, is retrieved using the time invariance in the repetitive experiment by selecting the field with the phase shift $e^{i(2\Omega_2 - \Omega_1)m\tau_r}$ from light reflected from the pillar. This is realized by measuring the spectrally resolved interference between a frequency shifted reference field with the phase $(2\Omega_2 - \Omega_1)m\tau_r$ and the signal from the sample. The delay between the pulse arrival times at the sample is denoted as τ, which is positive for $\mathcal{E}_1$ leading $\mathcal{E}_2$. The amplitude and phase of the FWM field are obtained via spectral interferometry [27]. More details of the experimental methodology and the corresponding notation are given in [16, 17, 28–30].

A major advantage of the FWM spectroscopy in measuring QSC is that in its lowest order it enables investigating the first two rungs of the JC ladder on an equal footing, accessing both the doublet of vacuum to first rung $0 \leftrightarrow M_{1\pm}$ transitions and the quadruplet of first to second rung $M_{1\pm} \leftrightarrow M_{2\pm}$ transitions, as depicted in figure 2. Moreover, the coherent evolution of the $0 \leftrightarrow M_{1\pm}$ and $0 \leftrightarrow M_{2\pm}$ transitions can be separately probed, employing distinct FWM creation pathways upon positive and negative delay τ. Details are given in the supplementary material of [16].

For $\tau > 0$ (see figure 2(a)), pulse $\mathcal{E}_1$ arrives first, inducing a one-photon coherence on $0 \leftrightarrow M_{1\pm}$, which after an evolution interval of τ is converted by pulse $\mathcal{E}_2$ in second order ($\mathcal{E}_2\mathcal{E}_2$) to FWM on both the doublet $0 \leftrightarrow M_{1\pm}$ and quadruplet $M_{1\pm} \leftrightarrow M_{2\pm}$. The FWM field $P(t, \tau)$, created at the arrival of $\mathcal{E}_2$, is proportional to the one-photon coherence on $0 \leftrightarrow M_{1\pm}$; thus the
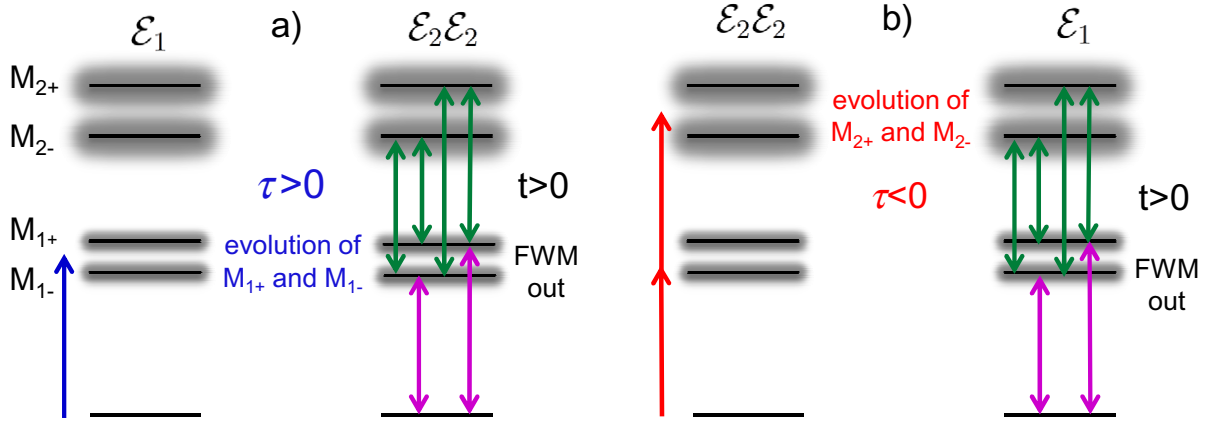
Figure 2. FWM creation pathways of order $\mathcal{E}_1^* \mathcal{E}_2^2$ within the JC ladder for different time ordering of the excitation pulses: (a) pulse $\mathcal{E}_1$ arrives first for $\tau > 0$ and (b) pulse $\mathcal{E}_2$ arrives first for $\tau < 0$.

delay-time dependence is measuring the coherent dynamics of the states $M_{1\pm}$. Here t is the real time, zero at the arrival of the second pulse. For $\tau < 0$ instead (figure 2(b)), pulse $\mathcal{E}_2$ arrives first, creating a two-photon coherence $\mathcal{E}_2 \mathcal{E}_2$ on the transitions to the second rung $0 \leftrightarrow M_{2\pm}$ which after an evolution interval of $-\tau$ is converted by the pulse $\mathcal{E}_1$ in first order to FWM on both the doublet $0 \leftrightarrow M_{1\pm}$ and quadruplet $M_{1\pm} \leftrightarrow M_{2\pm}$. The FWM polarization $P(t, \tau)$ is proportional to the two-photon coherence on $0 \leftrightarrow M_{2\pm}$; thus the delay-time dependence is measuring the coherent evolution of the states $M_{2\pm}$. Therefore, $P(t, \tau)$ decays and beats versus τ according to dephasing time and spectral splitting of $M_{1\pm}$ ($M_{2\pm}$), for $\tau > 0$ ($\tau < 0$), respectively. The time-resolved FWM $P(t, \tau)$ can also be represented as spectrally resolved FWM $\tilde{P}(\omega, \tau) = \int_0^\infty P(t, \tau) \mathrm{e}^{\mathrm{i}\omega t}\, \mathrm{d}t$, by transforming the real time t into the angular frequency ω.

We compare the measured FWM response with a theoretically modelled third-order polarization, calculated following our previous work [16]. The model is based on the Hamiltonian of the exciton–cavity system given by (in units of $\hbar$)

$$H = \omega_C a^\dagger a + \omega_X |1\rangle\langle 1| + g(a^\dagger |0\rangle\langle 1| + a |1\rangle\langle 0|) \tag{3}$$

with $a^\dagger$ and a denoting the creation and annihilation operators of the cavity photon and $|0\rangle$ and $|1\rangle$ the ground and excited states of the excitonic system, respectively. The density matrix $\rho(t)$ of such a system satisfies the master equation

$$\mathrm{i}\frac{\mathrm{d}\rho}{\mathrm{d}t} = \hat{L}\rho = [H, \rho] - \mathrm{i}\gamma_C(a^\dagger a\rho + \rho a^\dagger a - 2a\rho a^\dagger) - \mathrm{i}\gamma_X (|1\rangle\langle 1|\rho + \rho|1\rangle\langle 1| - 2|0\rangle\langle 1|\rho|1\rangle\langle 0|) \tag{4}$$

in which both cavity and exciton dissipation are taken into account in the standard Lindblad approach. We assume that the optical excitation and emission occur via the cavity photon mode. For ultrashort excitation pulses, the FWM polarization, i.e. the lowest-order term proportional to $\mathcal{E}_1^* \mathcal{E}_2^2$ in the total polarization of the system, is given by [31]

$$P(t, \tau) = \begin{cases} \mathrm{Tr}\left\{\mathrm{e}^{-\mathrm{i}\hat{L}t}\left[a^\dagger, \left[a^\dagger, \mathrm{e}^{-\mathrm{i}\hat{L}\tau}[a, \rho(-\infty)]\right]\right]a\right\} & \text{for} \quad \tau > 0, \\ \mathrm{Tr}\left\{\mathrm{e}^{-\mathrm{i}\hat{L}t}\left[a, \mathrm{e}^{\mathrm{i}\hat{L}\tau}\left[a^\dagger, [a^\dagger, \rho(-\infty)]\right]\right]a\right\} & \text{for} \quad \tau < 0. \end{cases} \tag{5}$$

IOP Institute of Physics   Φ DEUTSCHE PHYSIKALISCHE GESELLSCHAFT

In the above formulae the superoperator $\hat{L}$ defined in equation (4) is used, and $\rho(-\infty)$ denotes the density matrix before the optical excitation.

The FWM polarization is calculated by representing the Lindblad superoperator $\hat{L}$ as a matrix in the basis of uncoupled exciton and cavity states. For a system initially in the ground state, only the ground state and the first two rungs of the JC ladder, $M_{1\pm}$ and $M_{2\pm}$, are relevant in the lowest order of FWM. The FWM polarization is then given by

$$P(t, \tau) = \sum_{k=\pm} \sum_{j=1}^{6} c_{jk} \, e^{-i\tilde{\omega}_j t} \, e^{i\tilde{\lambda}_k \tau} \tag{6}$$

in which c_{jk} are constants calculated by matrix algebra, different for positive and negative delay times. The delay dynamics in equation (6) is given by the frequencies of the first rung $\tilde{\lambda}_\pm = \lambda_{1\pm}^*$ (second rung $\tilde{\lambda}_\pm = \lambda_{2\pm}$) for positive (negative) delay, where

$$\lambda_{n\pm} = \frac{(2n-1)(\omega_C - i\gamma_C) + \omega_X - i\gamma_X}{2} \pm \sqrt{\left(\frac{\omega_C - \omega_X - i\gamma_C + i\gamma_X}{2}\right)^2 + ng^2} \tag{7}$$

are the complex eigenfrequencies of the coupled exciton–cavity system. The real-time dynamics is given by complex frequencies of the six transitions

$$\begin{aligned}
&\tilde{\omega}_1 = \lambda_{1+}, \quad &\tilde{\omega}_3 = \lambda_{2+} - \lambda_{1+}^*, \quad &\tilde{\omega}_5 = \lambda_{2+} - \lambda_{1-}^*, \\
&\tilde{\omega}_2 = \lambda_{1-}, \quad &\tilde{\omega}_4 = \lambda_{2-} - \lambda_{1-}^*, \quad &\tilde{\omega}_6 = \lambda_{2-} - \lambda_{1+}^*,
\end{aligned} \tag{8}$$

between the ground state and the first rung ($\tilde{\omega}_{1,2}$), and the first and second rungs ($\tilde{\omega}_{3,4}$ and $\tilde{\omega}_{5,6}$) of the JC ladder. The parameters of the model used in this work have been determined from the photoluminescence characterization, as given in table 1 and described in section 2. Note that in the FWM calculation, the Lorentzian part of the spectrometer resolution of 4 μeV was included in real time but not in the delay-time dynamics.

4. Four-wave mixing results

4.1. Detuning dependence of four-wave mixing

The measured spectrally resolved FWM power $|\tilde{P}(\omega, 0)|^2$ as a function of the sample temperature T and the related detuning $\delta(T)$ is given in figure 3(a). We find that in the region close to zero detuning, no clear anti-crossing is observed, in contrast to the PL data of figure 1. This is caused by contributions of the second rung transitions $M_{1-} \leftrightarrow M_{2-}$ and $M_{1+} \leftrightarrow M_{2+}$, which are creating FWM signal in the spectral region between the first rung transitions.

The corresponding detuning dependence of the time-resolved FWM amplitude $|P(t, 0)|$ given in figure 3(c) shows a delayed rise and oscillations of the signal. This initial delay is caused by the coupling of the excitation pulses to the cavity photon, which is free from nonlinearity. Only when the corresponding initial superposition $M_{1+} + M_{1-}$ has evolved with time towards $M_{1+} - M_{1-}$ through the Rabi oscillation, does it acquire an excitonic component and FWM is created, which then has to be transferred back from the exciton to the cavity photon through the Rabi oscillation. The time evolution exhibits oscillations, which are given not only by the vacuum Rabi splitting of the first rung transitions, but also by the second rung transitions. The FWM rise time and oscillations are longest for $\delta = 0$, corresponding to the smallest frequency splitting of the six transitions in the JC ladder.
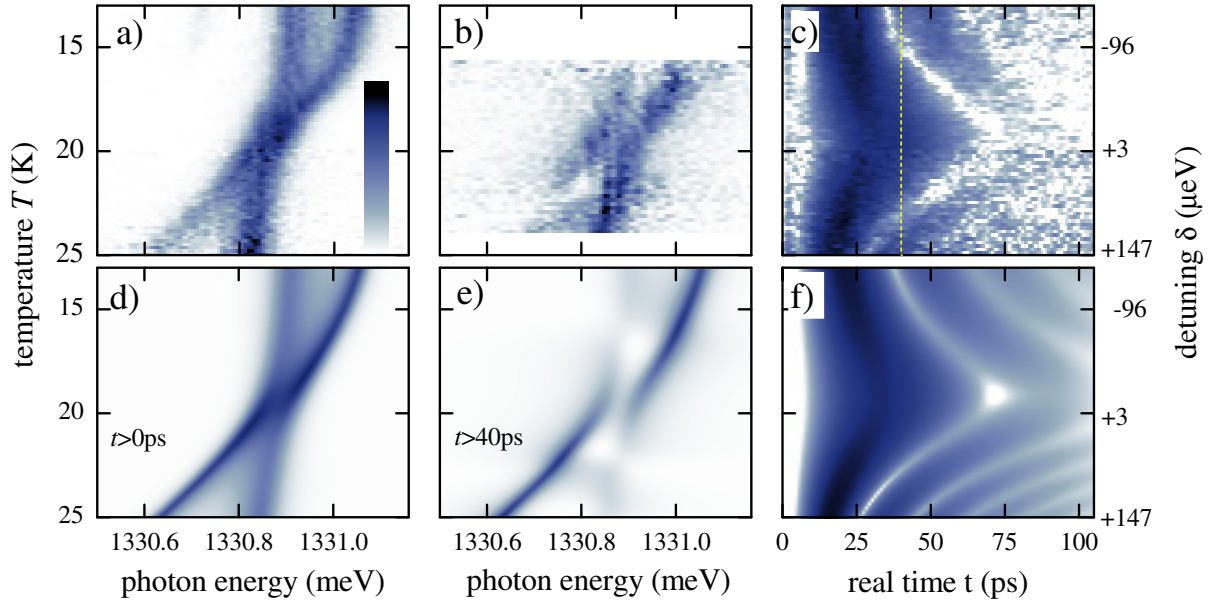
Figure 3. (a) The measured and (d) predicted FWM $|\tilde{P}(\omega, 0)|^2$ as a function of the temperature T and the corresponding detuning δ. Linear colour scale as shown in (a). (b) The measured and (e) predicted post-selected FWM $|\bar{P}_s(\omega, 0; 40\,\text{ps})|^2$. The post selection time $t_s = 40\,\text{ps}$ is shown in (c) as a dashed line. (c) The measured and (f) predicted FWM $|P(t, 0)|$. Logarithmic scale over three orders of magnitude as shown in (a). The data were normalized to their integral for each detuning.

Post-selecting the FWM signal emitted after a survival time t_s following its creation by the second pulse at $t = 0$ [16, 19], we can suppress the fast decaying components in the signal. In our case these are four second rung transitions $M_{1\pm} \leftrightarrow M_{2\pm}$, which have about three times faster decay times due to the higher photon content of the second rung, see equation (7). The post-selected FWM $\bar{P}_s(\omega, \tau; t_s) = \int_{t_s}^{\infty} P(t, \tau)\,e^{i\omega t}\,dt$ is therefore for sufficiently large t_s dominated by the first rung transitions $0 \leftrightarrow M_{1\pm}$, in accordance with equations (6)–(8). The resulting detuning dependence of $\bar{P}_s(\omega, \tau; 40\,\text{ps})$ is given in figure 3(b). $t_s = 40\,\text{ps}$ is indicated in figure 3(c) as a dashed line. The FWM is decreasing with increasing $|\delta|$, and is shown over the detuning range in which the post-selected FWM is above the noise. These data show an anti-crossing, as expected for the first-rung transitions, confirming that the system remains in strong coupling.

In figures 3(d)–(f), we present the theory predictions corresponding to figures 3(a)–(c). The predictions, which are based on the theoretical approach presented in section 3 and [16], are in good agreement with the measurements. All the salient features of the experimental data discussed above are reproduced.

4.2. Coherent dynamics on the first and the second rung of the Jaynes–Cummings ladder

As discussed in the previous section, the FWM for positive (negative) delay times gives access to the dynamics of the first (second) rung of the JC ladder, respectively, see equations (6)–(8). The measured delay-time dynamics is given in figure 4 for three different detunings δ. Close to
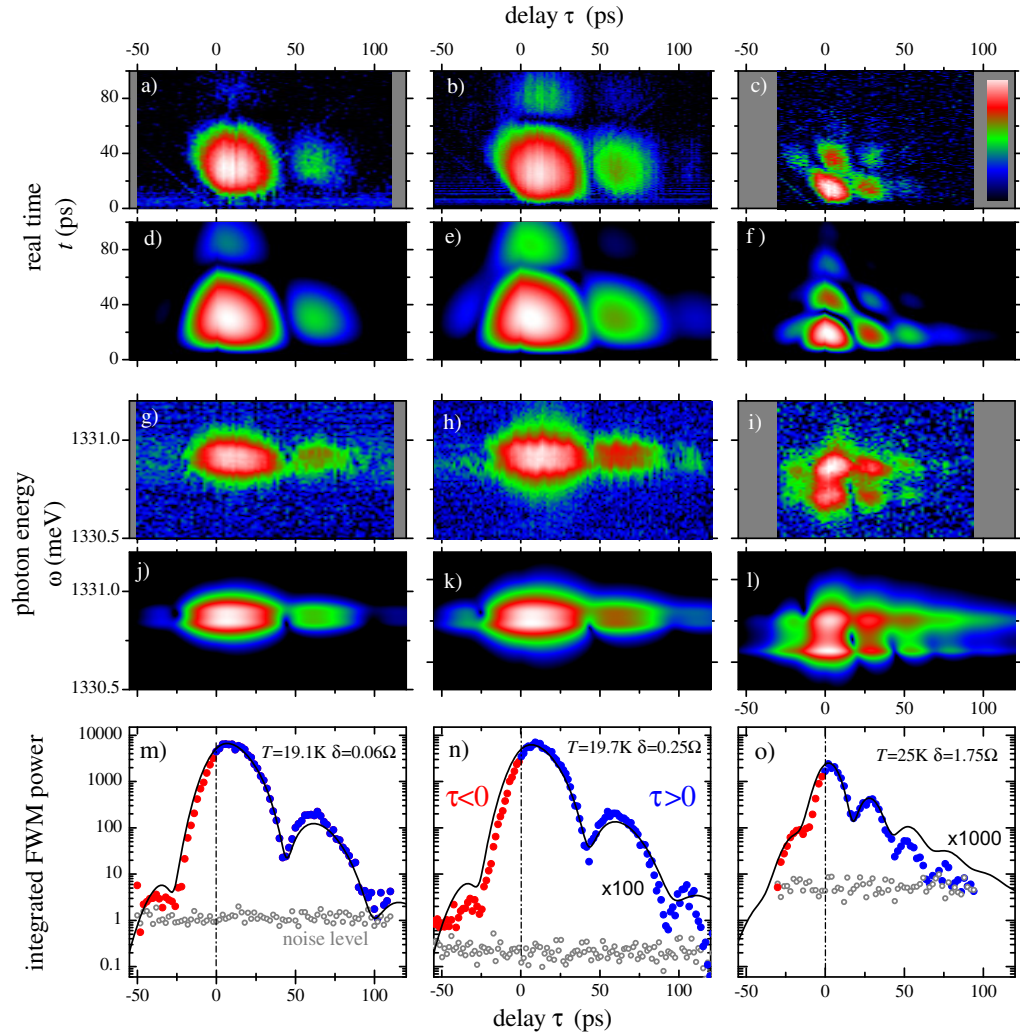
Figure 4. Delay-time dependence of the FWM for three different detunings $\delta = 0.06\,\Omega$ (left column), $\delta = 0.25\,\Omega$ (middle column) and $\delta = 1.75\,\Omega$ (right column). The excitation pulses $\mathcal{E}_1$ ($\mathcal{E}_2$) at the top facet of the micropillar had an energy of 0.03 fJ (0.08 fJ), 0.15 fJ (0.39 fJ) and 0.09 fJ (0.22 fJ), respectively. Top two rows: normalized time-resolved FWM $|P(t, \tau)|^2$, measured (a)–(c) and predicted (d)–(f). Logarithmic colour scale, given by the colour bar in (c), over 3, 4 and 2.5 orders of magnitude in (a), (d); (b), (e); and (c), (f), respectively. Middle two rows: spectrally resolved FWM $|\tilde{P}(\omega, \tau)|^2$, measured (g)–(i) and predicted (j)–(l). The same colour scale, logarithmic over 5 (4) orders of magnitude in (h); (g), (i). Dark grey areas indicate no data. Bottom row: (m)–(o) time-integrated power $|P|^2_{\mathrm{int}}(\tau)$, predicted (solid lines) and measured (filled circles, blue for $\tau > 0$ and red for $\tau < 0$). The units of the measured FWM power have been chosen to match the prediction at $\tau = 0$. The noise level of the measurement is gives as open circles.

zero detuning $\delta = 0.06\,\Omega$, the dynamics is the slowest. For $\tau > 0$, the time-integrated $|P|^2_{\mathrm{int}}(\tau) = \int_0^\infty |P(t, \tau)|^2\,\mathrm{d}t$ (see figure 4(m)) shows an exponential decay of about $T_2/2 = 2\tau_C = 21$ ps with a superimposed beat from the first rung with a period of 52 ± 2 ps, corresponding to a vacuum

Rabi splitting of $79 \pm 3\,\mu$eV, in agreement with the splitting measured in μPL. For $\tau < 0$ instead a much faster decay is observed. This is as expected, as the $M_{2\pm}$ states of the second rung (see figure 2(b)) have a photon content of $3/2$ compared to $1/2$ for the first rung at $\delta = 0$, and as a result a nearly three times faster decay rate, $T_2/2 = 2\tau_C/3 = 7$ ps. At $\delta \simeq 0$ the $M_{2\pm}$ states are expected to exhibit a $\sqrt{2}$ larger splitting than the $M_{1\pm}$ states, corresponding to a $\sqrt{2}$ shorter beat period of about 36 ps. In the measurements, we can observe the fast decay and a minimum around $\tau = -25$ ps. As for positive delay, the first minimum occurs somewhat earlier than one full period. The observation of this beat for $\tau < 0$, approximately $\sqrt{2}$ faster than for $\tau > 0$, is a direct manifestation of the second rung of the JC ladder and reveals the QSC regime. The theoretical prediction (solid lines) is in quantitative agreement for both positive and negative delays, supporting the interpretation of the data within the JC model. Specifically, the position of the minimum is consistent with the measurement, confirming the splitting of the second rung. Also, the time-resolved (figure 4(a)) and spectrally resolved (figure 4(g)) measurements and the corresponding theoretical predictions (figures 4(d) and (j)) are in agreement, including details of the spectral and temporal dynamics.

With increasing detuning, the dynamics becomes faster, as seen for $\delta = 0.25\,\Omega$ (figure 4, middle column) and $\delta = 1.75\,\Omega$ (figure 4, right column). The beat period is shortened as expected from larger splitting in all rungs given by $\sim \sqrt{n\Omega^2 + \delta^2}$, and the decay is modified due to a different photon content in the $M_{1\pm}$ and $M_{2\pm}$ states. Also here we find agreement between measurements and predictions.

We emphasize that for all three detunings reported here, we observe in $|P|^2_{\text{int}}(\tau)$ an oscillation at $\tau < 0$ given by the splitting in the second rung $M_{2\pm}$, with a dynamics in quantitative agreement with prediction. To observe this oscillation in the present sample, a dynamic range of at least two orders of magnitude in the FWM amplitude (four orders in the FWM power) was required. Previously reported data of this type (figure 4 of [16]) had insufficient dynamics to observe the minimum of the oscillation of the second rung at $\tau < 0$. The improved signal-to-noise ratio in the FWM measurements shown here was achieved by an improved detection efficiency of the heterodyne spectral interferometry setup (using a detector of higher saturation, readout rate and quantum efficiency (Princeton Instruments PIXIS:100BR), and by increasing the transmission in the detection path by optimized anti-reflection coatings) and the better characteristics of the present sample, including complete removal of the Ni hardmask during the etching of the micropillars. The sample employed in [16] suffered from a remaining Ni layer over the top facet of the micropillars, causing a reduction of the coupling efficiency.

4.3. Quantum-to-classical crossover of the strong coupling

The quantum-to-classical transition in the light–matter interaction has been first investigated in atomic physics in a double-pulse Ramsey interferometry setup [32]. By performing a complementarity experiment, it was demonstrated that the fringe contrast of a Ramsey interference (of Rydberg atoms strongly interacting with a coherent field in a low-loss cavity) increases for a mean photon number in a cavity changing from zero to around ten. This was followed by an investigation of strong coupling of an atom with a coherent field in a cavity containing several tens of photons [33]. The undefined photon number in such a mesoscopic field leads to a decay of Rabi oscillations, but using an echo technique this decay can be reversed,

showing the entanglement between atom and photon-number states. Recently, the quantum-to-classical transition of the strong coupling in a thermal field with increasing average phonon number was studied in superconducting qubits [34].

In this section, we investigate the quantum-to-classical crossover of the strong coupling regime in an exciton–cavity system [23]. It occurs when climbing the JC ladder until the change of the Rabi splitting between rungs $2(\sqrt{n+1} - \sqrt{n})g$ is much smaller than the linewidths. With varying the driving power of $\mathcal{E}_1$ and $\mathcal{E}_2$, we control the average number of injected photons into the cavity mode. In $\chi^{(3)}$ conditions corresponding to photon numbers below unity, we probe in FWM the first five levels of the JC ladder (the ground state and doublets in the first two manifolds), demonstrating the quantum character of strong coupling, as shown in the previous section. With increasing injected photon number, higher-order contributions involving higher rungs are dominating the FWM response. In the investigated structure, already the transitions from the second to third rung $M_{2\pm} \leftrightarrow M_{3\pm}$ have a shift of only $2(\sqrt{3} - \sqrt{2})g \sim 26 \, \mu$eV from the cavity mode, less than its width. Therefore, we reach the semi-classical regime of the strong coupling already in the third rung, with a spectral response expected to be similar to the Mollow triplet.

We investigate the crossover here at $\tau = 0$ and zero detuning. To give insight into the contributions of different rungs in the FWM response, we show in figure 5 the post-selected FWM spectra $|\bar{P}_s(\omega, 0; t_s)|^2$ for different post-selection times t_s and excitation powers. In the $\chi^{(3)}$ regime (left column), the FWM spectrum at $t_s = 0$ (figure 5(a1)) consists of contributions of the first and the second rung. The predicted decomposition of the signal into the first $0 \leftrightarrow M_{1\pm}$ (magenta line) and the second $M_{1\pm} \leftrightarrow M_{2\pm}$ (green line) rung contribution are given. The $0 \leftrightarrow M_{1\pm}$ transitions do show a vacuum Rabi doublet. The quadruplet $M_{1\pm} \leftrightarrow M_{2\pm}$ creates a spectrally broad peak due to faster dephasing. The coherent superposition of $0 \leftrightarrow M_{1\pm}$ and $M_{1\pm} \leftrightarrow M_{2\pm}$ yields the FWM spectral lineshape, given by the orange curve: with the current micropillar parameters, the six transitions form a shape with a small dip in the middle. The average excitation provided by $\mathcal{E}_1$ arriving at the top facet of the micropillar was 8 nW, corresponding to 0.1 fJ per pulse $\mathcal{E}_1$. From this, only 0.25% of light enter the cavity, considering the ratio between the ideal linewidth of the planar cavity without side-wall losses (6 μeV) and the pulse width of 2.5 meV. Taking into account a non-ideal mode matching by a factor of 0.8, we estimate that $\mathcal{E}_1$ ($\mathcal{E}_2$) injects into the photon mode, on average, 1 (2.5) photons per pulse. The measured spectrum, given by the shaded area, is in good agreement with the theoretical prediction in the $\chi^{(3)}$ limit.

Increasing the post-selection time t_s, as shown in figures 5(a2)–(a4), we can suppress the second rung contributions, as discussed earlier. For $t > 51$ ps the FWM is dominated by the $0 \leftrightarrow M_{1\pm}$ transitions, showing the expected Rabi-split doublet with a destructive interference in the centre. The predicted spectra confirm this interpretation.

Increasing the injected photon number of $\mathcal{E}_1$ to 2.5 and 10 and twice that for $\mathcal{E}_2$, the FWM spectra evolve as given in figures 5(b) and (c), respectively. These spectra are beyond the third-order regime and higher-rung transitions dominate the FWM. The resulting lineshape is a coherent superposition of all the transitions involved. With increasing n, the spectral positions of $M_{n\pm} \leftrightarrow M_{n+1\pm}$ transitions approach the cavity mode, and $M_{n\pm} \leftrightarrow M_{n+1\mp}$ are split to either side by the Rabi splitting $\sqrt{n}\Omega$, as seen in figure 5(c1), approaching the classical Mollow triplet [25].

In the post-selected spectra, with increasing t_s, higher rung contributions are sequentially reduced, until eventually only the first rung Rabi doublet remains. The system emits photons via the cavity loss; thus its state 'climbs down the JC ladder', i.e. the average photon number
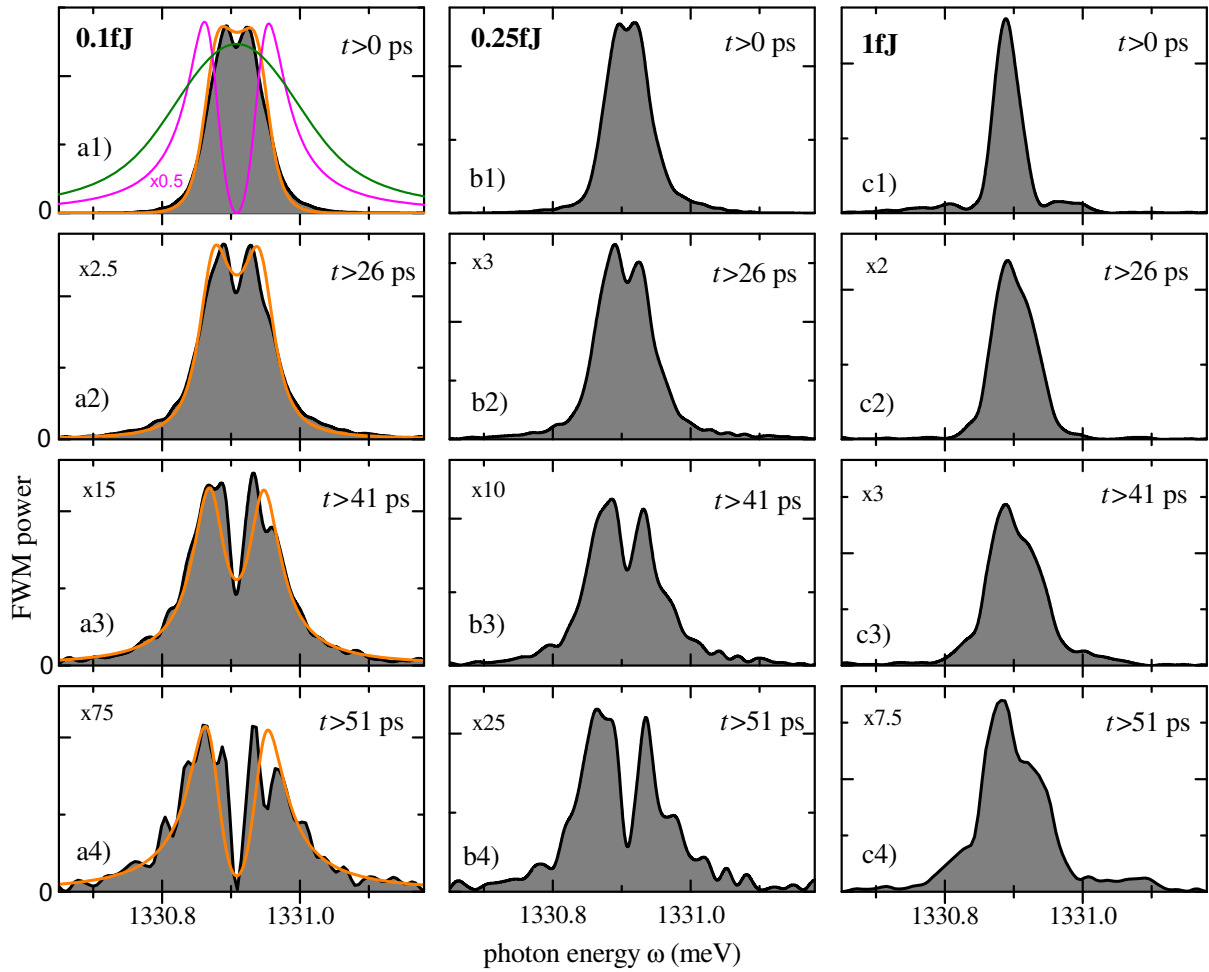
Figure 5. Post-selected FWM spectra $|\bar{P}_s(\omega, 0; t_s)|^2$ for different post-selection times $t_s = 0$, 26, 41 and 51 ps (from top to bottom) and excitation powers (left to right). Left column (a1)–(a4): excitation energy 0.1 fJ per pulse $\mathcal{E}_1$ corresponding to an estimated average of $n = 1$ injected photons. Middle columns (b1)–(b4): 0.25 fJ per pulse $\mathcal{E}_1$. Right column (c1)–(c4): 1 fJ per pulse $\mathcal{E}_1$. The relative scaling factors within each column are given. Orange lines: the predicted FWM spectra (normalized to data). A spectral decomposition into $M_{1\pm} \leftrightarrow M_{2\pm}$ transitions (green line) and $0 \leftrightarrow M_{1\pm}$ transitions (magenta line, multiplied by a factor of 0.5) is given in (a1).

decreases, going through a classical-to-quantum transition. The higher the initial excitation, the more the response is dominated by the higher rungs, i.e. the more the response looks like the semi-classical Mollow triplet. We note that observation of the Mollow triplet in FWM of an exciton–cavity system is substantially different from that observed in resonance fluorescence of quantum dots [35–37]. The latter corresponds to light scattering by a two-level system resonantly driven by a classical coherent field, while the former probes the free evolution within the JC ladder of a strongly coupled system after impulsive excitation, going through a classical-to-quantum transition.
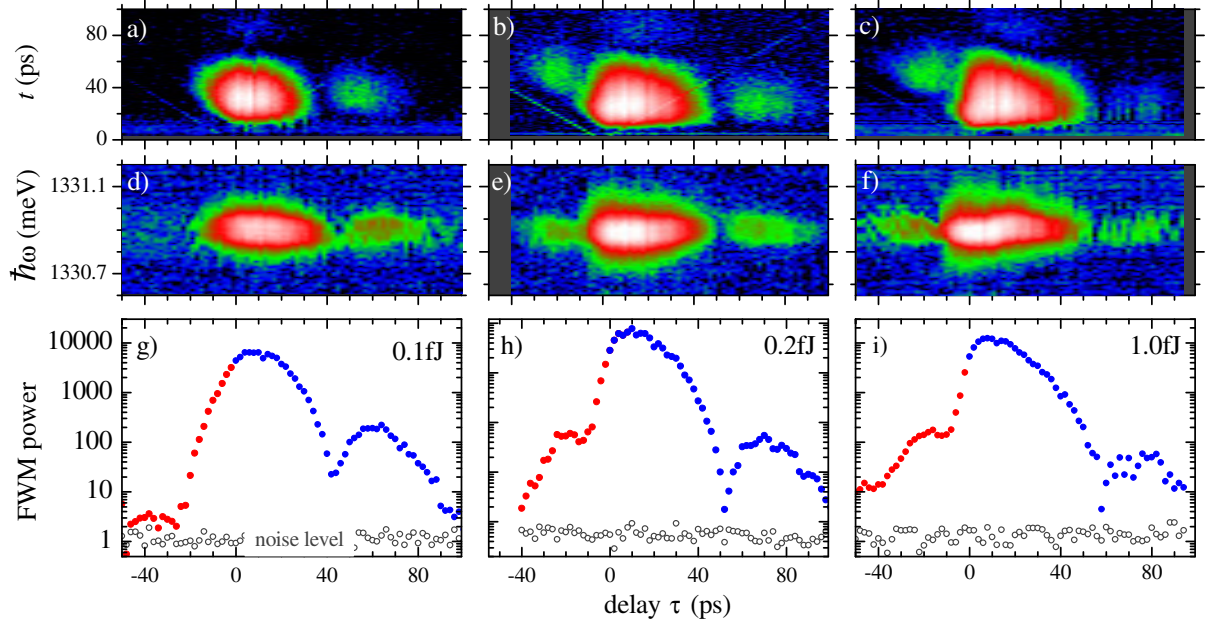
Figure 6. Measured delay-time-dependent FWM at $\delta = 0.06\,\Omega$ as a function of excitation fluence as indicated, for which an estimated average of one, two and ten photons are injected by the pulse $\mathcal{E}_1$ into the cavity in the left, middle and right columns, respectively. Top row: time-resolved FWM $|P(t,\tau)|^2$. Middle row: spectrally resolved FWM $|\tilde{P}(\omega,\tau)|^2$. Logarithmic colour scale as in figure 4 over three, four and five orders of magnitude in (a); (b), (c); and (d)–(f), respectively. Grey regions indicate no data. Bottom row: integrated FWM $|P|^2_{\text{int}}(\tau)$ in arbitrary units. The noise level of the measurement is given as open circles.

The delay-time dynamics with increasing injected photon number is shown in figure 6. The dynamics changes both for positive and for negative time delays. Specifically, the beat at negative delays reduces its period, as expected from the higher rungs, and gets less well defined as several rungs are contributing to the response. The spectral and real-time data show a more pronounced signal for $\tau < 0$. We tentatively attribute this observation to the transfer of the one-photon coherence for $\tau > 0$ to the second rung transitions $M_{1\pm} \leftrightarrow M_{2\mp}$ in a fifth-order process $\mathcal{E}_1\mathcal{E}_1^*\mathcal{E}_1^*\mathcal{E}_2^2$, which has a dephasing rate similar to the $0 \leftrightarrow M_{2\mp}$ two-photon coherence. A quantitative theoretical modelling of the FWM response including all relevant rungs of the JC ladder is at present being developed and will be reported in a forthcoming publication.

5. Conclusion

We have investigated the coherent response of an exciton–cavity system in the QSC regime using FWM. The dynamics of the first and the second rung has been measured and theoretically modelled, showing a quantum beat of the second rung about a factor of $\sqrt{2}$ shorter than the first rung. Increasing the number of injected photons, we observe the transition of the response towards a semiclassical Mollow triplet. Prospective FWM experiments on strongly coupled exciton–cavity systems with longer dephasing time could enable investigations of cQED effects

with mesoscopic fields [38] in solids, such as the demonstration of collapse and revival of Rabi oscillations.

Acknowledgments

References

[1] Brune M, Schmidt-Kaler F, Maali A, Dreyer J, Hagley E, Raimond J M and Haroche S 1996 *Phys. Rev. Lett.* **76** 1800–3

[2] Nogues G, Rauschenbeutel A, Osnaghi S, Brune M, Raimond J M and Haroche S 1999 *Nature* **400** 239–42

[3] Gleyzes S, Kuhr S, Guerlin C, Bernu J, Deléglise S, Hoff U B, Brune M, Raimond J M and Haroche S 2007 *Nature* **446** 297–300

[4] Fink J M, Goppl M, Baur M, Bianchetti R, Leek P J, Blais A and Wallraff A 2008 *Nature* **454** 315–8

[5] Hopfield J J and Thomas D G 1965 *Phys. Rev. Lett.* **15** 22–5

[6] Kaluzny Y, Goy P, Gross M, Raimond J M and Haroche S 1983 *Phys. Rev. Lett.* **51** 1175–8

[7] Weisbuch C, Nishioka M, Ishikawa A and Arakawa Y 1992 *Phys. Rev. Lett.* **69** 3314

[8] Brennecke F, Donner T, Ritter S, Bourdel T, Köhl M and Esslinger T 2007 *Nature* **450** 268–71

[9] Jaynes E and Cummings F 1963 *Proc. IEEE* **51** 89–109

[10] Bishop L S, Chow J M, Koch J, Houck A A, Devoret M H, Thuneberg E, Girvin S M and Schoelkopf R J 2009 *Nature Phys.* **5** 105–9

[11] Yoshie T, Scherer A, Hendrickson J, Khitrova G, Gibbs H M, Rupper G, Ell C, Shchekin O B and Deppe D G 2004 *Nature* **432** 200–3

[12] Faraon A, Fushman I, Englund D, Stoltz N, Petroff P and Vuckovic J 2008 *Nature Phys.* **4** 859–63

[13] Volz T, Reinhard A, Winger M, Badolato A, Hennessy K J, Hu E L and Imamoğlu A 2012 *Nature Photon.* **6** 605–9

[14] Peter E, Senellart P, Martrou D, Lemaître A, Hours J, Gérard J M and Bloch J 2005 *Phys. Rev. Lett.* **95** 067401

[15] Reithmaier J P, Sęk G, Löffler A, Hoffmann C, Kuhn S, Reitzenstein S, Keldysh L V, Kulakovskii V D, Reinecke T L and Forchel A 2004 *Nature* **432** 197–200

[16] Kasprzak J, Reitzenstein S, Muljarov E A, Kistner C, Schneider C, Strauss M, Höfling S, Forchel A and Langbein W 2010 *Nature Mater.* **9** 304–8

[17] Langbein W and Patton B 2006 *Opt. Lett.* **31** 1151

[18] Kasprzak J, Reitzenstein S, Muljarov E, Kistner C, Schneider C, Strauß M, Höfling S, Forchel A and Langbein W 2010 *Proc. SPIE* **7600** 760015

[19] Albert F *et al* 2013 *Nature Commun.* doi:10.1038/ncomms2764

[20] Reitzenstein S and Forchel A 2010 *J. Phys. D: Appl. Phys.* **43** 033001

[21] Pässler R *et al* 1999 *J. Appl. Phys.* **86** 4403–11

[22] Laucht A, Hauke N, Villas-Bôas J M, Hofbauer F, Böhm G, Kaniber M and Finley J J 2009 *Phys. Rev. Lett.* **103** 087405

[23] del Valle E and Laussy F P 2011 *Phys. Rev.* A **84** 043816

[24] Borri P, Langbein W, Woggon U, Stavarache V, Reuter D and Wieck A 2005 *Phys. Rev.* B **71** 115328

[25] del Valle E and Laussy F P 2010 *Phys. Rev. Lett.* **105** 233601

IOP Institute of Physics **Φ** DEUTSCHE PHYSIKALISCHE GESELLSCHAFT

[26] Münch S, Reitzenstein S, Franeck P, Löffler A, Heindel T, Höfling S, Worschech L and Forchel A 2009 *Opt. Express* **17** 12821–8

[27] Lepetit L, Chériaux G and Joffre M 1995 *J. Opt. Soc. Am.* B **12** 2467

[28] Langbein W 2010 *Riv. Nuovo Cimento* **33** 255–312

[29] Langbein W and Patton B 2007 *J. Phys.: Condens. Matter* **19** 295203

[30] Kasprzak J, Patton B, Savona V and Langbein W 2011 *Nature Photon.* **5** 57–63

[31] Muljarov E A and Zimmermann R 2006 *Phys. Status Solidi* b **243** 2252–6

[32] Bertet P, Osnaghi S, Rauschenbeutel A, Nogues G, Auffeves A, Brune M, Raimond J M and Serge H 2001 *Nature* **411** 166–70

[33] Auffeves A, Maioli P, Meunier T, Gleyzes S, Nogues G, Brune M, Raimond J M and Haroche S 2003 *Phys. Rev. Lett.* **91** 230405

[34] Fink J M *et al* 2010 *Phys. Rev. Lett.* **105** 163601

[35] Ates S, Ulrich S M, Reitzenstein S, Löffler A, Forchel A and Michler P 2009 *Phys. Rev. Lett.* **103** 167402

[36] Vamivakas A N, Zhao Y, Lu C Y and Atatüre M 2009 *Nature Phys.* **5** 198–202

[37] Flagg E B, Muller A, Robertson J W, Founta S, Deppe D G, Xiao M, Ma W, Salamo G J and Shih C K 2009 *Nature Phys.* **5** 203–7

[38] Meunier T, Gleyzes S, Maioli P, Auffeves A, Nogues G, Brune M, Raimond J M and Haroche S 2005 *Phys. Rev. Lett.* **94** 010401